Stratigraphy of St Audrie's Bay

The TJB section studied at St. Audrie's Bay, UK, spans the Rhaetian age Westbury and Lilstock Formations through to the Hettangian (Angulata Zone) of the Blue Lias Formation (Hesselbo et al., 2004; Hounslow et al., 2004; Ruhl et al., 2010) (Fig DR1). Globally, the TJB is defined by the first appearance of the ammonite species *Psiloceras spelae*, in the GSSP section, Austria (von Hillebrandt et al., 2007). The first *Psiloceras* species that occur at St Audrie's Bay (*P.* cf. *erugatum* and *P. planorbis*) are, however, younger than *P. spelae* (von Hillebrandt et al., 2007), and the TJB must therefore be lower in the section. The first appearance of the pollen taxon *Cerebropollenites thiergartii* also marks the TJB (von Hillebrandt et al., 2007), and at St Audrie's Bay this taxon first occurs within the Pre-Planorbis Zone, just below the first occurrence of *Psiloceras* (Bonis et al., 2010). The remaining Blue Lias Formation contains abundant ammonites that provide a biostratigraphic framework through the Jurassic (Fig. DR1) (Hesselbo et al., 2004; Mander et al., 2008).

Position of the Late Triassic Extinction Horizon

Although a few taxa have their last regional occurrences at the boundary between the Lilstock Formation and the overlying Blue Lias Formation, all of the taxa that become globally extinct have their last occurrences within a short stratigraphic interval spanning the uppermost Westbury Formation to lower Lilstock Formation (Mander et al., 2008), just below the first negative carbon isotope excursion (Hesselbo et al., 2004) (Fig. DR1). Studies of sampling and preservational biases suggest that, for the bivalves at least, this extinction event is real, and not an artefact of the rock and fossil records (Mander and Twitchett, 2008). The upper Cotham and lower Langport members are almost devoid of benthic macrofossils and have been interpreted as a post-extinction 'Dead Zone' (Mander et al., 2008). Post-extinction recovery was complete by the Angulata Zone of the Hettangian (Barras and Twichett, 2007; Mander et al., 2008).

Correlation of the Extinction Event with Changes in Atmospheric pCO$_2$

The TJB atmospheric pCO$_2$ record is derived from analysis of plant fossil cuticle from a site in East Greenland (McElwain et al., 1999; Steinthorsdottir et al., 2011). Published correlations between St Audrie's Bay and East Greenland have been made from detailed palynological and stable isotopic analyses (Belcher et al., 2010; Mander et al., 2013). These published correlations have been used in this study to correlate the pCO$_2$ data with our samples. Although these correlations are robust around the extinction event and TJB, the precise point at which pCO$_2$ values return to pre-extinction levels within the Hettangian is less constrained, and herein we

follow the correlation of (Belcher et al., 2010). It is possible that the return to pre-extinction levels of $p\text{CO}_2$ occurred as early as the base of the Planorbis Zone or as late as the Angulata Zone.

Additional $p\text{CO}2$ data were recently published from analyses of soil carbonates of the Newark Basin (Schaller et al., 2011). The good magnetostratigraphic record at St Audrie's Bay (Hounslow et al., 2004), enables correlation with these sections in the Newark Basin (Deenen et al., 2010). This correlation demonstrates that the lowest CAMP basalts correlate with the extinction event (Deenen et al., 2010; Mander et al., 2013), although the resolution is not good enough to precisely correlate individual paleosol horizons of (Schaller et al., 2011) with our samples. Thus, we have used the better correlated East Greenland data of (McElwain et al., 1999) and (Steinthorsdottir et al., 2011) to provide a comparative $p\text{CO}_2$ record in this study.
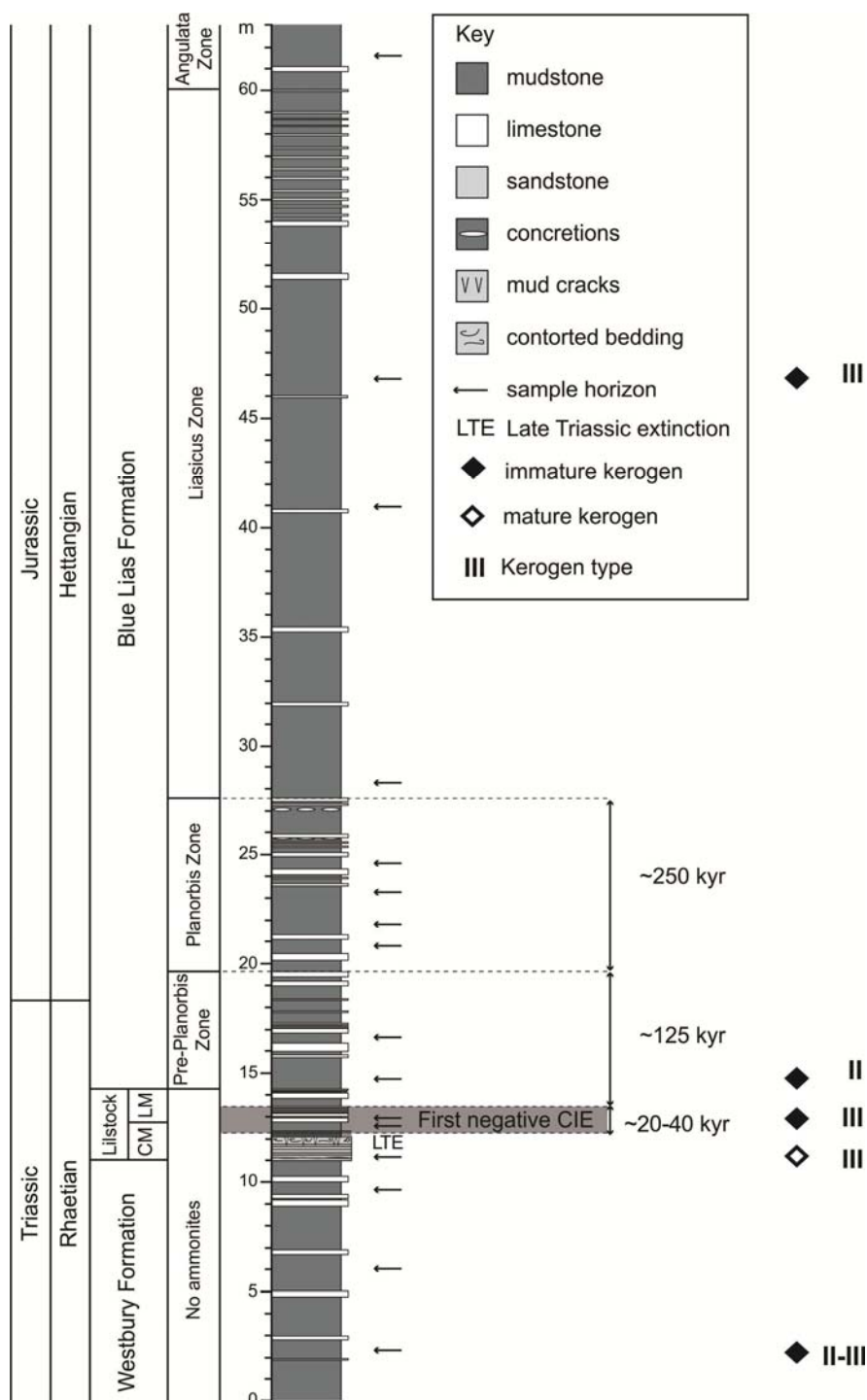
Figure DR1. Stratigraphic log of St. Audrie's Bay outcrop, showing sampled horizons. Ammonite zonation is from (Hounslow et al., 2004); estimated durations of time intervals around the TJB are derived from an astronomical timescale (Ruhl et al., 2010); positions of TJB and extinction event are discussed in the text; the identifications of kerogen type and maturity derive from analyses discussed in the text.

Methods

Crushed sub-samples were sonicated in methanol (MeOH), dichloromethane (DCM) and hexane (10 minutes each). When dry, the samples were powdered. About 40 to 80 g powders were extracted with DCM: MeOH (9:1 *v/v;* 72 hr) using a Soxhlet apparatus. Elemental sulfur was removed using activated copper, filtered and the remaining extract dried under a constant stream of N_2. The extracts were weighed and aliquots (70 mg) were pre-adsorbed onto activated silica gel. This was added onto a silica gel column (20 cm length x 2.5 cm diameter) pre-washed with *n*-hexane. Then saturate hydrocarbons were eluted using (40 mL) *n*-hexane, aromatic hydrocarbons with 8:2 (*v/v*) hexane:DCM , 1:1 (*v/v*) *n*-hexane: DCM to elute nickel porphyrin fractions, DCM for the elution of vanadyl porphyrins, 9.5:1 (*v/v*) DCM: acetone to elute maleimides and 1:1 (*v/v*) DCM: MeOH for eluting the polar fraction. For this paper, only the saturated and aromatic fraction results are presented. To achieve better chromatography of the saturated fraction, the *n*-alkanes were separated from the branched and cyclic compounds by using an activated (250 ° C, 12 hr) 5Å molecular sieve (Dawson et al., 2005).

A split/splitless injector of a 6890 gas chromatograph (GC) interfaced to HP 5973 mass selective detector. The column used was a DB-5MS (60 m), consisting of 5% phenylmethylsiloxane and helium was used as the carrier gas (1 mL/min). The GC oven was set at 40 °C and increased at 3 °C/min to 310 °C (30 min). Masses were scanned from 50 to 500 Daltons. To quantify, aliquots of the saturated and aromatic fractions were spiked with squalane and perdeuterated terphenyl, respectively.

Aliquots up to 90% of the saturated (including branched and cyclic) and aromatic fractions were analyzed by CSIA using an Isoprime GC-isotope ratio mass spectrometer (GC-IRMS). The GC oven program for the saturated fraction was the same to that used for the GC-MS analyses, but for the aromatics the final temperature was raised to 320 °C (30 min). Helium was used as the carrier gas (1.5 ml/min) and the column used was a DB-5MS (60 m; J&W Scientific). The furnace was heated to 850 °C. Water was removed cryogenically with liquid nitrogen (maintained at -100 °C). Values are reported in ‰ relative to Vienna Peedee Belemnite standard. Two or three replicates were conducted and the average and standard deviation, when applicable, were reported.

Bulk $\delta^{13}C$ of kerogen was measured using Delta V Plus mass spectrometer connected with a Thermo Flush 112 via Conflo IV. To acquire OM of bulk kerogen, carbonates were removed from the extracted rock powder with 10% hydrochloric acid (HCl) added dropwise. For $\delta^{13}C$ of carbonate, the samples were individually prepared in a fully automated acid dosing system using anhydrous phosphoric acid to dissolve only the carbonates. The samples were then analyzed in a GasBenchII coupled with a Delta XL Mass Spectrometer. The external error of δ13C analyses is ~0.10 ‰.

Bulk $\delta^{34}S$ values of total sulfur were analyzed on sediment powders representing a mixture of essentially reduced inorganic and organic sulfur. $^{34}S/^{32}S$ ratios were measured as described by (Dodson et al., 1974) by means of combustion isotope-ratio monitoring mass spectrometry (C-irmMS) using a Thermo Finnigan MAT 253 mass spectrometer coupled to a Thermo scientific Flash 2000 elemental analyser via a Thermo Scientific Conflo IV split interface. V_2O_5 was used as catalyst. The stable sulfur isotope value was calibrated with in-house and international reference materials (IAEA-S-1, -2, -3) and are reported in the conventional δ-notation relative to the Vienna Canon Diablo Troilite (VCDT) standard. Duplicate measurements agreed within ±0.3‰.

Sedimentary inorganic sulfur (essentially pyrite) was extracted by a one-step distillation procedure with acidic hot chromium(II) chloride solution (Fossing and Jorgensen, 1990). Hydrogen sulfide was quantitatively fixed in zinc acetate solutions and transformed into Ag_2S. After washing and drying of the samples, solids were combusted with added V_2O_5 as a catalyst, and $^{34}S/^{32}S$ ratios measured as described in (Jørgensen et al., 2004; Grice et al., 2005).

Table DR1. Rock-eval pyrolysis data

| Sample | Elevation (m) | Formation | Rock Eval | | | | Tmax (°C) | HI | OI | S2/S3 | S1/TOC *100 | PI[†] |
			TOC (%)	S1*	S2**	S3***						
LIA 4 AB	35	LIA	0.34	0.04	0.47	0.65	434	137	189	0.7	12	0.08
LIAS-1 AB	14.5	Blue Lias	2.91	0.41	18.83	1.05	426	648	36	17.9	14	0.02
Lang-1AB	12	Lilstock	0.29	0.00	0.28	0.71	433	97	247	0.4	0	0
C-2 AB	11	Lilstock	0.03	0.00	0.09	0.63	550	360	2520	0.1	0	0
W1-AB	1.5	Westbury	1.64	0.19	4.42	0.51	427	269	31	8.7	12	0.04

Total Organic Carbon, TOC (wt %)
*Volatile hydrocarbon content (mg HC/mg rock)
**Remaining HC generative potential (mg HC/mg rock)
***CO_2 content (mg CO_2/mg rock)
[†] Production Index = S1/ (S1+S2)
Hydrogen Index, HI = S2 x 100/TOC
Oxygen Index, OI = S3 x 100 / TOC, mg CO_2 / g TOC

The Cotham Member of the Lilstock Formation has T_{max} 550 °C indicating post mature OM and has the lowest TOC. This coke-like residual organic carbon is consistent with a larger rock-eval suite of Lilstock Formation samples from the Doniford Bay section (Paris et al., 2010). This sample is from a shallow water setting, and the biomarkers deposited in this environment have likely undergone extensive degradation compared to biomarkers in the overlying Langport Member as well as in Westbury and Blue Lias Formations.
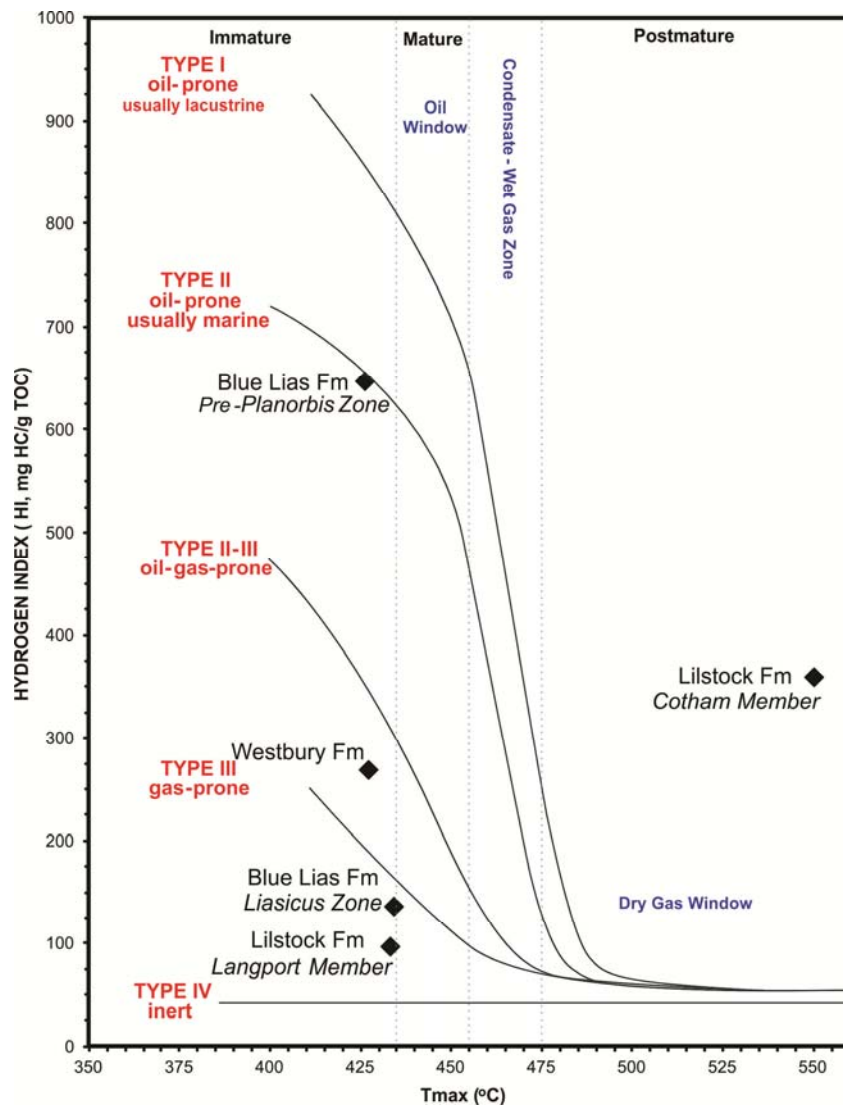
Figure DR2. Van Krevelen diagram

Table DR2. Abundances of biological markers

Sample	elevation	Aryl isoprenoids			Algal		leaf wax			Pr/Ph	AIR	
		C_{16}	C_{18}	Iso	Pristane	Phytane	$n\text{-}C_{27}$	$n\text{-}C_{29}$	$n\text{-}C_{31}$		Free	S-bound
	m											
A1	61.6	na	na	na	0.6879	0.5138	3.1179	2.1127	0.4837	1.34	na	na
LIA4	46.8	0.0061	0.0038	nd	0.0027	0.0018	0.0569	0.0834	0.0567	1.51	2.29	na
P4	24.6	0.3890	0.4460	0.0247	0.6630	0.8558	8.3121	12.5330	6.2804	0.77	1.18	0.12
P3	23.2	0.2430	0.2901	0.0226	1.6698	2.5462	3.0303	3.9180	2.0194	0.66	0.82	na
P1	20.8	5.3127	8.0143	3.0472	2.4334	3.9272	22.4476	39.9883	9.7234	0.62	0.88	na
LIAS-2	16.6	7.3743	10.6414	3.7536	60.3111	62.1374	55.2046	93.0072	73.2070	0.97	1.16	na
LIAS-1	14.8	0.6719	1.4062	1.9774	1.2920	2.9239	12.2017	22.1757	13.4586	0.44	0.31	0.07
LANG1	12.9	0.0114	0.0038	nd	0.0532	0.0506	1.4832	1.5698	0.7524	1.05	3.89	nd
C2	12.6	nd	nd	nd	0.0061	0.0134	15.1153	9.3416	3.9894	0.46	nd	na
C1	11.1	nd	nd	nd	0.0138	0.0080	1.9908	1.2545	0.6698	1.72	nd	na
W6	9.7	nd	0.0515	nd	9.4696	6.2586	5.0101	5.1621	2.6611	1.51	nd	na
W1	2.3	nd	nd	nd	0.8807	0.6442	6.4308	6.2846	4.5992	1.37	nd	na

Abundances in µg/g rock; nd=not detected; na=not analysed

Table DR3. Stable carbon and sulfur isotope data

Sample	elevation	Aryl isoprenoids			isoprenoids		*n*-alkane		trophic indicator (C17+18)$_{ave}$-(Pr+Ph)$_{ave}$	Kerogen		Bulk	
		C$_{16}$	C$_{18}$	Iso	Pristane	Phytane	*n*-C$_{19}$	*n*-C$_{29}$		organic matter	carbonate	TRIS	TS
	m	δ^{13}C	δ^{13}C	δ^{13}C	δ^{13}C	δ^{13}C	δ^{13}C	δ^{13}C	δ^{13}C	δ^{13}C	δ^{13}C	δ^{34}S	δ^{34}S
A1	61.6									-29.8	-0.1	-27.8	-37.1
LIA4	46.8						-33.9*	-29.6			-2.4		
LIA3	41.2									-30.8	-1.0	-37.8	-33.1
LIA2	32.4										-0.2		
LIA1	28.2									-30.9		-27.4	-22.7
P5	26.7										-3.0		
P4	24.6	-22.4	-22.4		-33.9	-34.3	-35.8	-32.3	-2.5	-35.4	-1.3	2.3	5.7
P3	23.2				-34.6	-34.9	-35.1	-30.7			-1.1		
P2	21.9									-31.4		-17.9	-11.6
P1	20.8	-19.8	-18.8		-33.6	-33.0	-34.9	-31.5	-3.2	-30.5	-0.6	-8.3	-3.6
LIAS-3	19.3									-30.8		-18.0	-11.4
LIAS-2	16.6				-33.0	-31.5	-36.6	-32.8*			1.0		
LIAS-1	14.8	-16.2	-15.5	-13.5	-30.2	-28.8	-33.3	-29.6	-3.8	-26.8	-0.3	-24.6	-18.7
LANG1	12.9				-34.2	-33.9*	-37.6	-35.2	-2.9	-30.1	-3.0	-20.2	-20.1
C1	11.1							-30.4		-25.2	-2.9	-11.3	-5.8
W6	9.7				-33.4	-33.5	-31.3	-28.3	-0.5	-26.4	-2.4	-14.6	-17.1
W4	6									-26.7	-2.6	-20.3	-22.6
W1	2.3				-33.7*	-33.8*	-31.8	-32.7	1.4	na	na	2.4	-2.1

δ^{13}C in ‰ versus Vienna Pee Dee Belemnite; δ^{34}S in ‰ versus Vienna Canyon Diablo Troilite; TRIS=total reduced iron sulfide; TS=total sulfur; values are average of two measurements unless indicated (*) for one measurement
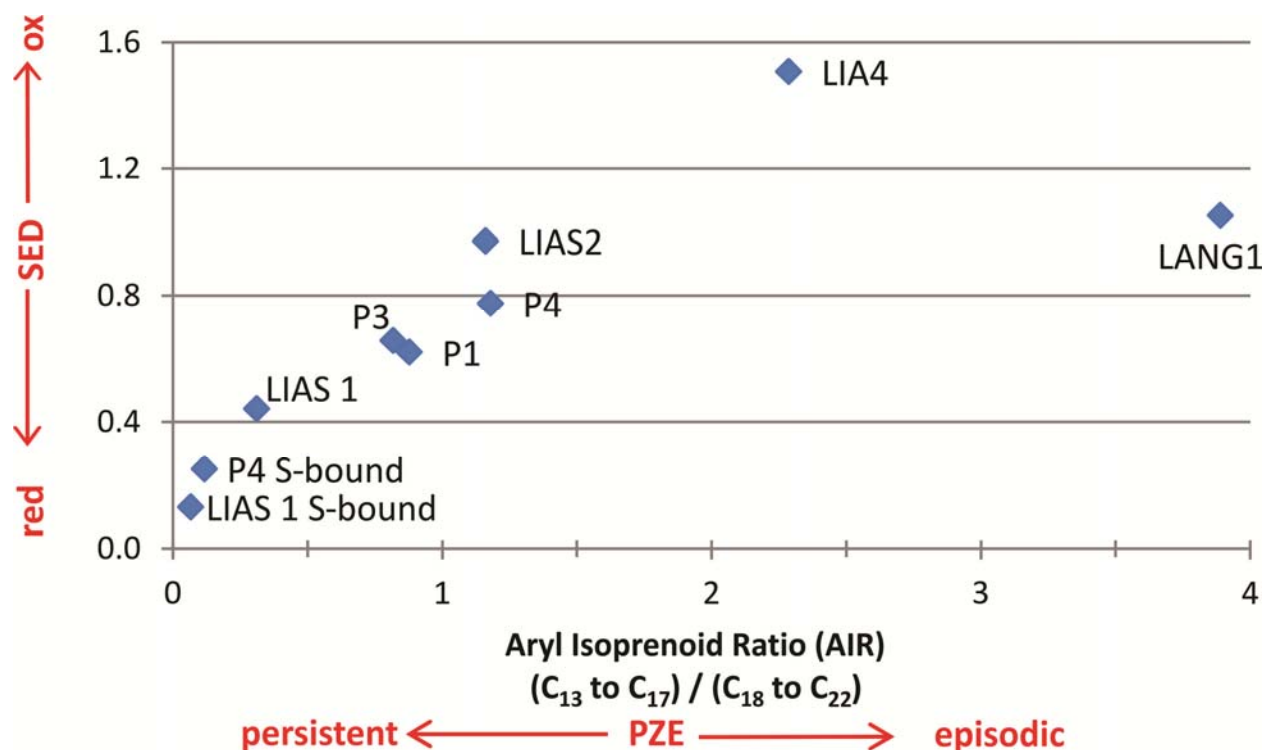
Figure DR 3. The Aryl Isoprenoid Ratio (AIR) was formulated from the Lower Jurassic Dotternhausen Posidonia Shale to compare the shorter-chain (C_{13} to C_{17}) from the longer-chain moieties as oxic degradation of isorenieratane produces shorter aryl isoprenoids (*19*). Persistent water column euxinia is expressed in AIR values <0.5 and short-term phases reach 3. AIR and molecular redox indicator Pr/Ph categorize persistent PZE during deposition of LIAS 1. Raney-Nickel catalyst desulfurization performed on the polar fractions of bitumens also show persistent PZE for LIAS 1 and P4 samples.

Sulfur Isotopes

To isolate factors that perturb biogeochemical cycles, such as the changes in OM type, marine and terrestrial kerogen are analyzed separately. Pyrite $\delta^{34}S$ records a strong negative correlation with Type II kerogen $\delta^{13}C$ (r^2=-0.78) from the Pre-Planorbis and Planorbis Zones and a positive correlation with the Type III kerogen $\delta^{13}C$ (r^2=0.69) from the Westbury Formation and Angulata Zone of the Blue Lias Formation (Fig. DR4A and B). There is also a strong linear inverse relationship between pyrite $\delta^{34}S$ and the leaf wax $\delta^{13}C$ (Fig DR4B) and algal biomarkers (Fig. DR4C). The results for kerogen II and algae may indicate the combined effect of climate change and an increase of ^{12}C in the water column with sulfate limitation during sediment deposition, leading to a reservoir effect for dissolved sulfate and/or an enhanced pyrite burial rate.
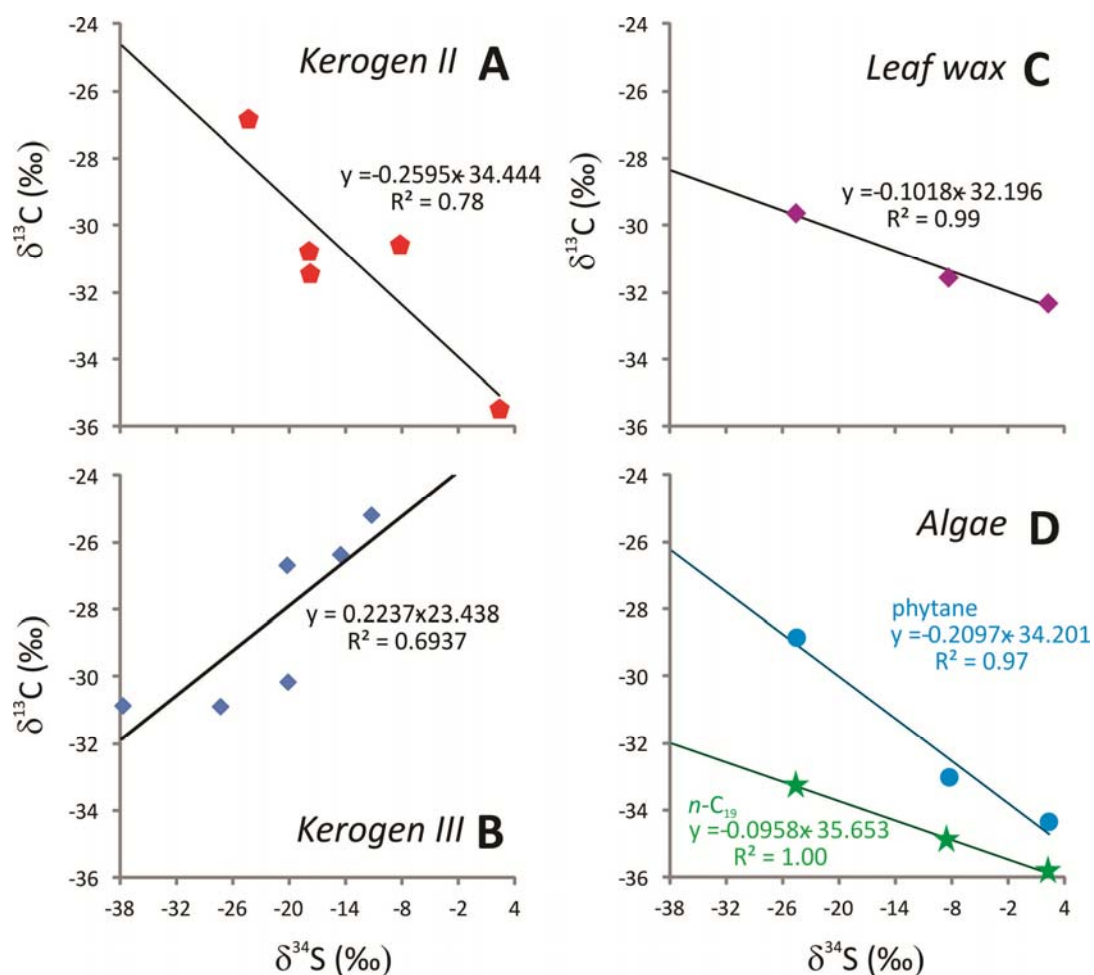
Figure DR4. Linear relationships of pyrite $\delta^{34}S$ to $\delta^{13}C$ of (A) kerogen II, (B) kerogen III, (C) leaf wax, and (D) algae.

REFERENCES

Barras, C. G., and Twichett, R. J., 2007, Response of the marine infauna to Triassic-Jurassic environmental change: Ichnological data from southern England: Palaeogeography Palaeoclimatology Palaeoecology, v. 244, p. 223-241.

Belcher, C. M., Mander, L., Rein, G., Jervis, F. X., Haworth, M., Hesselbo, S. P., Glasspool, I. J., and McElwain, J. C., 2010, Increased fire activity at the Triassic/Jurassic boundary in Greenland due to climate-driven floral change: Nature Geoscience, v. 3, no. 6, p. 426-429.

Bonis, N. R., Ruhl, M., and Kurschner, W. M., 2010, Milankovitch-scale palynological turnover across the Triassic-Jurassic transition at St. Audrie's Bay, SW UK: Journal of the Geological Society, v. 167, no. 5, p. 877-888.

Dawson, D., Grice K, and Alexander, R., 2005, Effect of maturation on the indigenous δD signatures of individual hydrocarbons in sediments and crude oils from the Perth Basin (Western Australia): Organic Geochemistry, v. 36, p. 95-104.

Deenen, M. H. L., Ruhl, M., Bonis, N. R., Krijgsman, W., Kuerschner, W. M., Reitsma, M., and van Bergen, M. J., 2010, A new chronology for the end-Triassic mass extinction: Earth and Planetary Science Letters, v. 291, no. 1-4, p. 113-125.

Dodson, R. G., Needham, R. S., Wilkes, P. G., Page, R. W., Smart, P. G., and Watchman, A. L., 1974, Uranium mineralization in the Rum Jungle-Alligator Rivers Province, Northern Territory, Australia, *in* Proceedings Formation of uranium ore deposits, Athens, Greece, May 6-10 1974, IAEA, p. 750.

Fossing, H., and Jorgensen, B. B., 1990, Isotope Exchange-Reactions with Radiolabeled Sulfur-Compounds in Anoxic Seawater: Biogeochemistry, v. 9, no. 3, p. 223-245.

Grice, K., Cao, C. Q., Love, G. D., Bottcher, M. E., Twitchett, R. J., Grosjean, E., Summons, R. E., Turgeon, S. C., Dunning, W., and Jin, Y. G., 2005, Photic zone euxinia during the Permian-Triassic superanoxic event: Science, v. 307, no. 5710, p. 706-709.

Hesselbo, S. P., Robinson, S. A., and Surlyk, F., 2004, Sea-level change and facies development across potential Triassic-Jurassic boundary horizons, SW Britain: Journal of the Geological Society, v. 161, p. 365-379.

Hounslow, M. W., Posen, P. E., and Warrington, G., 2004, Magnetostratigraphy and biostratigraphy of the Upper Triassic and lowermost Jurassic succession, St. Audrie's Bay, UK: Palaeogeography, Palaeoclimatology, Palaeoecology, v. 213, no. 3–4, p. 331-358.

Jørgensen, B. B., Böttcher, M. E., Lüschen, H., Neretin, N., and I., V., 2004, Anaerobic methane oxidation and a seep H2S sink generate isotopically heavy sulfides in Black Sea sediments: Geochimica et Cosmochimica Acta, v. 68, p. 2095-2118.

Mander, L., Kürschner, W. M., and McElwain, J. C., 2013, Palynostratigraphy and vegetation history of the Triassic–Jurassic transition in East Greenland: Journal of the Geological Society, v. 170, no. 1, p. 37-46.

Mander, L., and Twitchett, R. J., 2008, Quality of the Triassic-Jurassic Bivalve Fossil Record in Northwest Europe: Palaeontology, v. 51, p. 1213-1223.

Mander, L., Twitchett, R. J., and Benton, M. J., 2008, Palaeoecology of the Late Triassic extinction event in the SW UK: Journal of the Geological Society, v. 165, no. 1, p. 319-332.

McElwain, J. C., Beerling, D. J., and Woodward, F. I., 1999, Fossil Plants and Global Warming at the Triassic-Jurassic Boundary: Science, v. 285, no. 5432, p. 1386-1390.

Paris, G., Beaumont, V., Bartolini, A., Clemence, M. E., Gardin, S., and Page, K., 2010, Nitrogen isotope record of a perturbed paleoecosystem in the aftermath of the end-Triassic crisis, Doniford section, SW England: Geochemistry Geophysics Geosystems, v. 11.

Ruhl, M., Deenen, M. H. L., Abels, H. A., Bonis, N. R., Krijgsman, W., and Kurschner, W. M., 2010, Astronomical constraints on the duration of the early Jurassic Hettangian stage and recovery rates following the end-Triassic mass extinction (St Audrie's Bay/East Quantoxhead, UK): Earth and Planetary Science Letters, v. 295, no. 1-2, p. 262-276.

Schaller, M. F., Wright, J. D., and Kent, D. V., 2011, Atmospheric Pco2 Perturbations Associated with the Central Atlantic Magmatic Province: Science, v. 331, no. 6023, p. 1404-1409.

Steinthorsdottir, M., Jeram, A. J., and McElwain, J. C., 2011, Extremely elevated CO2 concentrations at the Triassic/Jurassic boundary: Palaeogeography, Palaeoclimatology, Palaeoecology, v. 308, no. 3–4, p. 418-432.

von Hillebrandt, A., L., K., and Kuerschner, W. M., 2007, A candidate GSSP for the base of the Jurassic in the Northern Calcareous Alps (Kuhjoch section, Karwendel Mountains, Tyrol, Austria): International Subcommission on Jurassic Stratigraphy Newsletter, v. 34, no. 1, p. 2-20.